ADVANCED ENGINEERING MATERIALS
www.aem-journal.com

Biodegradable, Self-Adhesive, Stretchable, Transparent, and Versatile Electronic Skins Based on Intrinsically Hydrophilic Poly(Caproactone-Urethane) Elastomer

Pulikanti Guruprasad Reddy, Vipul Sharma, Vijay Singh Parihar,* Ijlal Haider, Amit Barua, Anastasia Koivikko, Kyriacos Yiannacou, Hatai Jongprasitkul, Minna Kellomäki, and Veikko Sariola*

In biomedical sciences, there is a demand for electronic skins with highly sensitive tactile sensors that have applications in patient monitoring, human–machine interfaces, and on-body sensors. Sensor fabrication requires high-performance conductive surfaces that are transparent, breathable, flexible, and easy to fabricate. It is also preferable if the electrodes are easily processable as wastes, for example, are degradable. In this work, the design and fabrication of hydrophilic silanol/amine-terminated poly(caprolactone-urethane) (SA-PCLU) elastomer-based breathable, stretchable, and biodegradable electrodes are reported. Ag nanowires dispersed in water are sprayed onto the intrinsically hydrophilic electrospun SA-PCLU that became embedded into the scaffold and formed conformal hydrophilic polyurethane-based conductive networks (HPCN). The electrodes are used to fabricate capacitive, curvature, and strain sensors, all having monomaterial composition. In addition to displaying particularly good transparencies at low sheet resistances, stretchability, hydrophilicity, and tight and conformal bonding with the target surface, the electrodes also allow the evaporation of perspiration, making them suitable for epidermal sensors for long-time use. The application of the HPCN electrodes in flexible electronics and bionic skin applications is demonstrated through gesture monitoring experiments and swelling sensors.

1. Introduction

With the recent rapid progress in wearable electronic sensor technology real-time human motion monitoring, smart prosthetics, active patient biofeedback, and advanced bionic skins are increasingly becoming available.[1–3] Recently, various flexible/stretchable materials and devices have been continuously developed, such as flexible transistors, highly sensitive pressure sensors, high-resolution integrated circuits, stretchable functional electrodes, circuitries, and artificial skins.[4–7] Especially, flexible tactile sensors with high performances have achieved significant breakthroughs for various practical applications, which are based on different physical transduction mechanisms, including piezo resistivity, capacitance, and piezoelectricity.[8,9] However, it remains a significant challenge to develop a highly stretchable transparent tactile sensor with large-scale integration and rapid response time. These types of sensors are very useful for gait monitoring in individuals suffering from neurological ailments such as Huntington's disease,[10] multiple sclerosis,[11] Parkinson's disease,[12] and other associated neurological conditions. These sensors can provide very useful information regarding the development of disease. The constant monitoring of gait features can facilitate early diagnosis and biofeedback and lead to patient-specific treatment strategies.[13] There is a need for inexpensive, flexible, stretchable, skin-mountable, breathable, and eco-friendly sensors that allow the precise monitoring of human movement and other physiological parameters like posture, breathing, muscle tremors, gait, and limb movements. There are conventional semiconductor and metal foil-based sensors available in the market that have limited flexibility, low resolution, and ease of use, especially in human joint movements.[14] To increase the flexibility, resolution, and range of sensing, nanomaterial-elastomer composites based on flexible strain and capacitive pressure sensors have been reported for wearable devices.[15]

P. G. Reddy, V. Sharma, I. Haider, A. Barua
Department of Mechanical and Materials Engineering
University of Turku
20014 Turku, Finland
E-mail: vipul.sharma@utu.fi

V. S. Parihar, I. Haider, A. Koivikko, K. Yiannacou, H. Jongprasitkul, M. Kellomäki, V. Sariola
Faculty of Medicine and Health Technology
Tampere University
Korkeakoulunkatu 3, 33720 Tampere, Finland
E-mail: vijay.parihar@tuni.fi

The ORCID identification number(s) for the author(s) of this article can be found under https://doi.org/10.1002/adem.202401704.

DOI: 10.1002/adem.202401704

To create sensors capable of withstanding bending, twisting, and stretching, it is essential to develop a skin-like conductive surface that functions as an electrode. Several elastomeric synthetic polymers, such as silicon-based elastomers (e.g., polydimethylsiloxane (PDMS), Dragon Skin, Ecoflex, and Sylgard), thermoplastic polyurethane (TPU), and styrene-ethylene-butylene-styrene (SEBS), are commonly used as traditional stretchable substrates for fabricating skin-like conductive surfaces due to their exceptional mechanical properties.[16–19] Recently, several synthetic biodegradable polymers and gels,[20] self-healing materials,[21] and ionic conducting elastomers[22] have emerged as promising alternatives to traditional stretchable substrates for advanced wearable devices. On the other hand, various conductive nanomaterials, including silicon nanoribbons, carbonaceous materials, and metallic nanowires, have been employed to create polymer-based stretchable conducting surfaces.[23] Researchers have developed ultrathin, stretchable, and compliant epidermal electrodes by creating specific structural configurations such as a "wavy" herringbone layout,[24,25] "pop-up" wave geometry,[26] and a filamentary "serpentine" mesh.[27,28] Silver nanowire and polymer composites are particularly attractive for their properties. Robust, transparent, and breathable epidermal electrodes have been reported, consisting of a scaffold-reinforced conductive nanonetwork made of Ag nanowires and TPU[29]/polyamide (PA)[30]/polyacrylonitrile (PAN).[31] However, polymer-nanowire-based epidermal electrodes for use in sensors are facing significant challenges. First, electrodes fabricated from traditional polymeric substrates suffer from sustainability concerns due to their nondegradability.[17,32] Second, the hydrophobic nature of traditional polymeric substrates makes it difficult to attach conductive Ag nanowires to the substrate surfaces when water is used as the solvent during the fabrication process.[33] Therefore, it is essential to develop novel polymeric elastomers that are internally hydrophilic, allowing them to adhere to Ag nanowires and create mechanically robust conductive surfaces, while also being biodegradable. On the other hand, using normal flexible electrodes with substrates suffers from breathability issues, which can affect wearability comfort and skin health due to the lack of thermal and moisture management between the electrode and the human skin. While substrate-free electrodes provide a solution, their robustness and durability are often sacrificed, and the conductive material is needed in bulk.[34]

Furthermore, most previously reported epidermal electrodes are opaque and visible on the skin, which limits their uses for circumstances requiring a high level of optical transmission.[35,36] Therefore, it is highly desirable to develop a type of highly robust, breathable, and transparent electrode that has a strong bond with the skin for conformal interactions.[37] There is a pressing need for cost-efficient methods to produce nanomaterial fillers that would facilitate further development, rapid prototyping, and subsequent commercialization of inexpensive yet highly sensitive and reliable devices for human motion monitoring applications. Hence, the next-generation sensors must be skin-mountable noninvasive, lightweight, yet inexpensive to facilitate widescale applicability. The artificial skin-like sensors can pave the way for next-generation human motion monitoring, human–machine interface devices, and myoelectric prostheses.

In this work, we demonstrate the fabrication of biodegradable, breathable, transparent, and flexible tactile sensors based on hydrophilic amine-terminated polycaprolactone elastomer using an electrospinning technique. Ag nanowires dispersed in the water were evenly assembled on the hydrophilic amine-terminated polycaprolactone elastomer nanofiber surface using the air spray method. An optical transmittance of ≈80% was achieved at a low sheet resistance of 10 $\Omega\,sq^{-1}$. The stretchability and robustness of the film are demonstrated using the stress–strain tests. The uniformity of the Ag nanowire network across the surface is attributed to the hydrophilicity induced by the functional groups within the polymer. Due to the strong van der Waals force of the nanofibers,[38] the conducting film displays a uniform and conformal attachment with diverse types of target surfaces, including the skin. Owing to the porous structure for air conduction, the conducting film allows the evaporation of perspiration, making it suitable as an epidermal electrode for long-term use. The conducting surfaces were used to fabricate the capacitive pressure sensor, curvature sensor, and stain sensor in the single-component system where only one polymer is used. The sensors are fully degradable, and the single-component system makes the process facile. Surfaces based on hydrophilic polyurethane may pave the way for the fabrication of degradable and sophisticated functional electronic skins for various sensing applications.

2. Results and Discussion

Scheme 1 illustrates the synthetic route for the hydrophilic SA-PCLU elastomer, obtained through a two-step synthetic approach. Initially, poly(caprolactone-isophorone) diisocyanate is synthesized via a urethane reaction between poly(caprolactone) diol and isophorone diisocyanate in a 1:2 M ratio at 80 °C under a nitrogen atmosphere and solvent-free conditions for 3 h. This is followed by a reaction with the chain extender triethylene glycol (TEG) in the presence of a dibutyltin dilaurate (DBTDL) catalyst in dry DMF for 2 h at the same reaction temperature, leading to poly(caprolactone-urethane) diol as a starting prepolymer. In the second step, the hydrophilic SA-PCLU elastomer is synthesized through the silanization of poly(caprolactone-urethane) diol with (3-aminopropyl)triethoxysilane (APTES), followed by the hydrolysis of the silyl-ether functional group. The synthesized SA-PCLU elastomer was thoroughly characterized using IR and NMR analysis.

In the main polymer chain of the elastomer, the poly(caprolactone) and poly(TEG) molecular chains act as soft segments, while the urethane molecular chains act as hard segments. The combination of these segments is responsible for contributing to the physicochemical properties of the elastomer. For example, the soft segments in the elastomer offer flexibility and stretchability. Additionally, they contribute to degradability properties. The ester functionality in the soft segments is labile towards hydrolytic degradation in aqueous conditions as well as other enzymatic conditions, thus contributing to the degradability of the elastomer.[39] This property makes the synthesized elastomer an environmentally responsible choice for use as a substrate for fabricating flexible devices. On the other hand, the urethane hard segments contribute mechanical properties such as hardness and toughness to the elastomer. The novelty of the elastomer design involves the introduction of

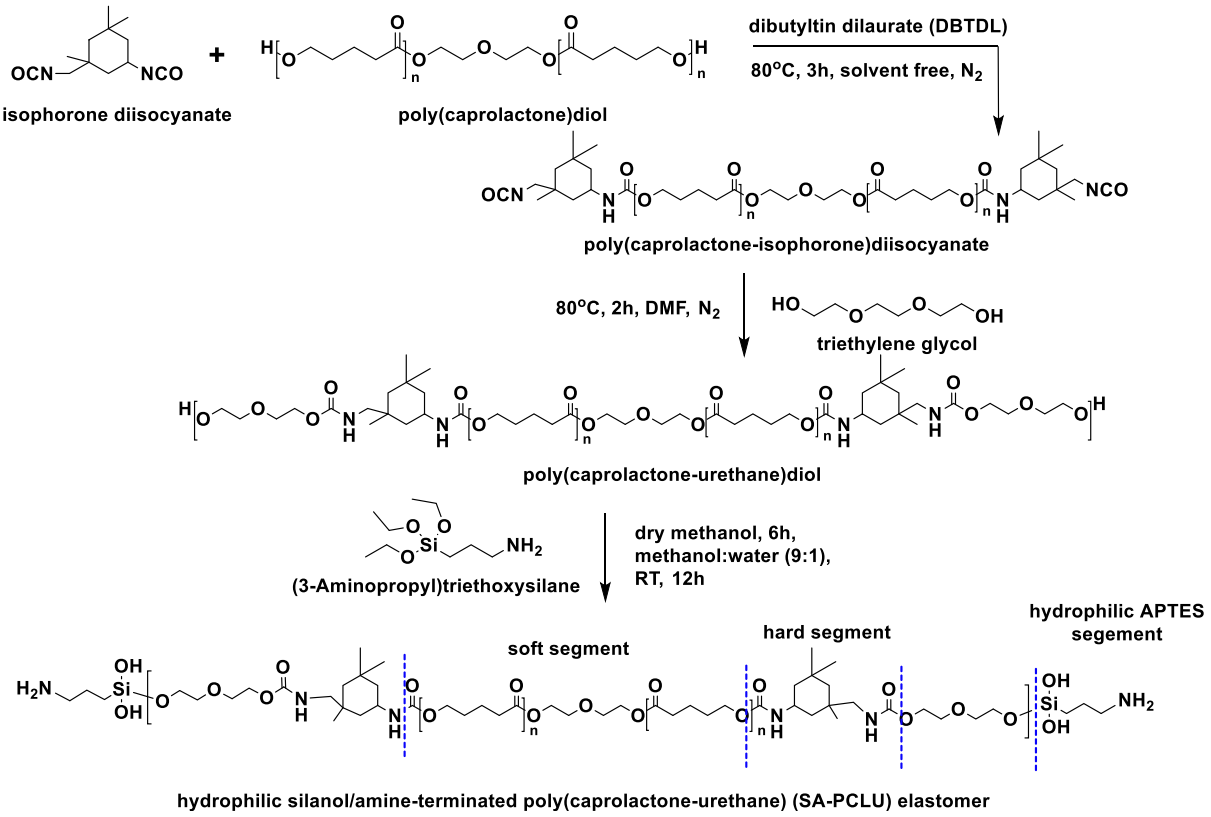

Scheme 1. Synthetic route for hydrophilic SA-PCLU elastomer.

silanol/amine functionality using APTES in the polymer terminal segments to enhance the wettability of the polymer by making it more hydrophilic (Scheme 1). Conventional methods to introduce hydrophilicity in polyurethane-based elastomers mostly involve surface treatments,[40,41] but this approach has several limitations, such as hydrophilicity being limited to the surface and reduced elasticity of the native polyurethanes. Recently, to enhance the surface wettability of our developed sustainable cross-linked poly(glycerol-co-δ-valerolactone) urethane substrates, we introduced an innovative method involving the incorporation of electrospun poly(vinyl alcohol) as a temporary wet film leveling layer on the substrate surface.[42] This approach facilitated improved adhesion of Ag nanowires to the substrate, enabling the fabrication of mechanically robust transparent conducting electrodes. In some silicon-based elastomeric substances, such as PDMS, the hydrophilicity is not stable after plasma treatment, as it can revert to being hydrophobic upon storage in dry air.[43] The hydrophobic recovery of the PDMS substrates upon storage in dry air after exposure to plasma and corona discharge was well studied using contact angle measurements.[44,45] In our method, the hydrophilic silanol/amine functionality of APTES was covalently integrated as terminal end groups into the elastomer chain. Therefore, the hydrophilicity of the elastomer is not limited to the surface and does not affect the polymer's elasticity and flexibility.[29,30] There are a few methods that have made the overall polymer surface hydrophilic by plasma treatment,[46] but the long-term hydrophilicity and the uniformity of the functional material attachment are not very good.

To confirm the APTES segment as a terminal hydrophilic end chain in the SA-PCLU elastomer, FTIR spectroscopy was employed. **Figure 1**a shows the FTIR profile of the SA-PCLU elastomer compared with the prepolymer poly(caprolactone-urethane) diol and the control poly(caprolactone) diol. The bands in the range of 1528–1537 cm^{-1} correspond to N–H deformation in both the SA-PCLU and poly(caprolactone-urethane) diol. The broad band observed at 3362 cm^{-1} is attributed to the stretching vibrations of –Si-OH and $–NH_2$ functional groups in the APTES segment of SA-PCLU, indicating the hydrophilic nature of the elastomer. In contrast, this peak is absent in the control poly (caprolactone) diol, which instead displays a peak at a higher wavenumber (3535 cm^{-1}) due to terminal hydroxyl groups in its structure. Additionally, a distinctive peak at 1038 cm^{-1} indicates the stretching vibrations of Si–O functionalities (silanols) in the elastomer,[47] which is not seen in both the poly(caprolactone-urethane) diol and the control poly(caprolactone) diol. This confirms the presence of the hydrophilic APTES segment in SA-PCLU. The existence of APTES in SA-PCLU was also further confirmed by proton NMR spectroscopy. The NMR peaks were assigned based on the chemical structure of SA-PCLU by comparing them with those of the prepolymer poly(caprolactone-urethane) diol and the control poly(caprolactone) diol, as shown in Figure 1b. The proton NMR spectrum of SA-PCLU displayed resonance peaks for APTES methylene and NH_2 protons at

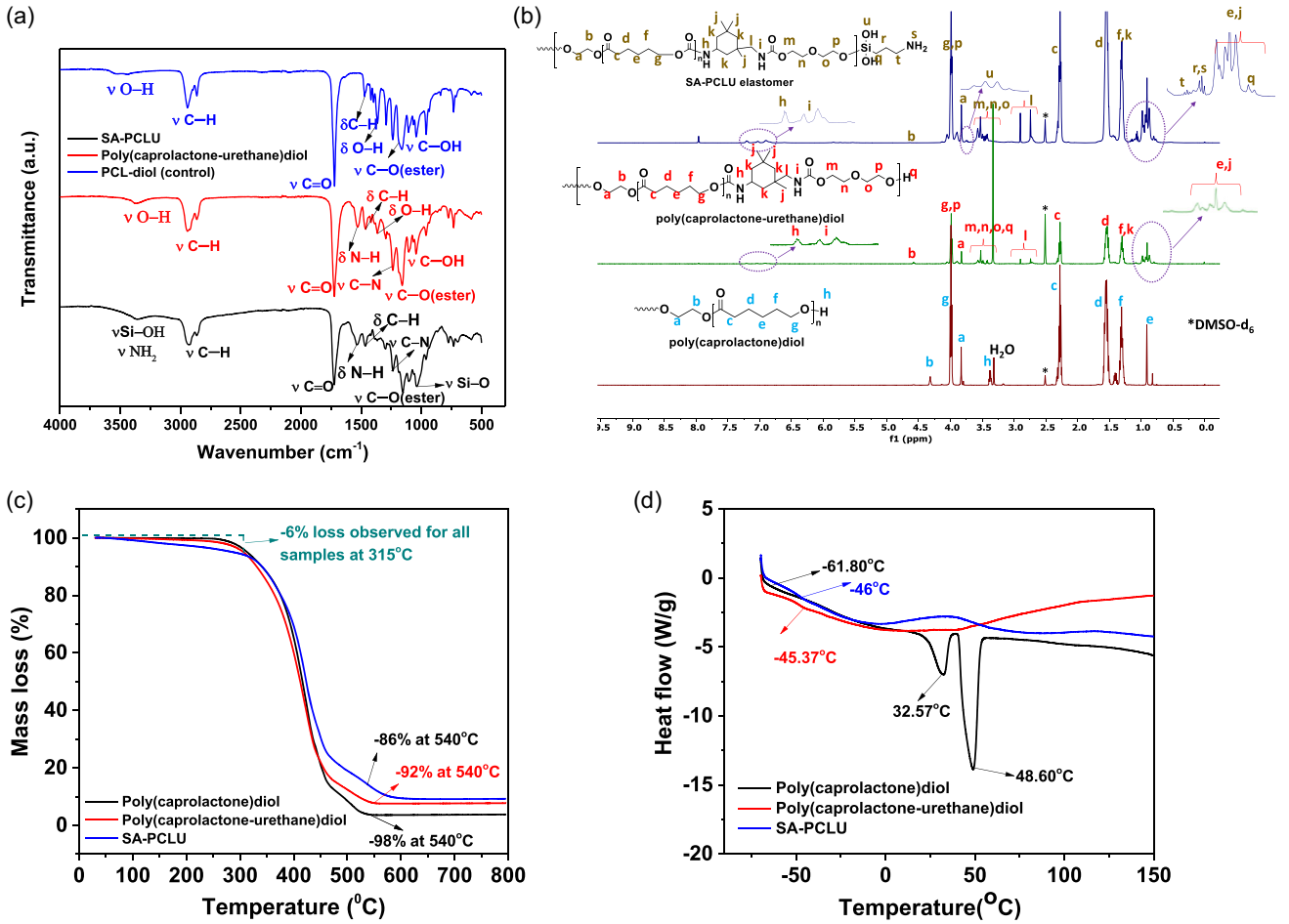

Figure 1. Characterization of hydrophilic SA-PCLU elastomer with the comparison of prepolymer poly(caprolactone-urethane) diol and the control poly(caprolactone) diol. a) FT-IR data, b) NMR data, c) TGA data, and d) DSC data.

1–1.25 ppm, while silanol groups appeared at 3.75 ppm.[48] Additionally, resonance peaks observed in the range of 6.75–7.25 ppm for SA-PCLU and its prepolymer correspond to urethane linkage NH protons[49] in their polymer's main chain. These resonance peaks are absent in the control poly(caprolactone) diol, confirming the formation of hydrophilic SA-PCLU.

To investigate the thermal properties such as glass transition temperature (T_g) and melting temperature (T_m) of SA-PCLU, in comparison with the prepolymer poly(caprolactone-urethane) diol and the control poly(caprolactone) diol, we subjected the samples to TGA and DSC analysis (Figure 1c,d). TGA analysis showed that all these polymers are thermally stable at 300 °C and exhibited an initial mass loss of 6% at 315 °C. The control polymer showed almost 98% mass loss at 540 °C, while only 92% loss was observed for the poly(caprolactone-urethane) diol and 86% for SA-PCLU at the same temperature, indicating their higher thermal stability. The leftover residual mass ≈10% observed for SA-PCLU beyond 590 °C is likely due to the remaining inorganic Si-O residue from APTES (Figure 1c). On the other hand, DSC studies show that both the prepolymer and SA-PCLU exhibited T_g values of −45 °C and −46 °C, respectively, while the control poly(caprolactone) diol displayed T_g at −61 °C (Figure 1d). In addition, due to its crystalline nature, the control poly(caprolactone) diol displayed two sharp T_m peaks at 32 °C and 48 °C, while these peaks were absent in SA-PCLU and the prepolymer poly(caprolactone-urethane) diol, indicating their amorphous nature due to elasticity.

Figure 2 shows a pictorial presentation of the fabrication of hydrophilic polyurethane-based conductive network (HPCN) electrodes and the layout for typical capacitive pressure and strain sensors. To fabricate the HPCN electrode, the electrospun SA-PCLU film was used as a flexible, stretchable, and transparent substrate (refer to the experimental section, Table S1 and Video SV1, Supporting Information, for electrospinning details). The hydrophilic surface of the SA-PCLU, mounted onto a 3D-printed frame (50 × 50 mm), was air sprayed with diluted Ag nanowires (100 μg mL^{-1}, aspect ratio = 70 nm × 40 μm) in water to make the surface conductive. The use of Ag nanowires dispersed in organic solvents was avoided in this study, as they tend to dissolve the SA-PCLU elastomers (see Figure S1, Supporting Information). During spraying, the Ag nanowires in water were delivered as numerous small droplets. Upon landing on the SA-PCLU substrate surface, they underwent uniform dispersion across the substrate due to its high wettability, caused by hydrophilic

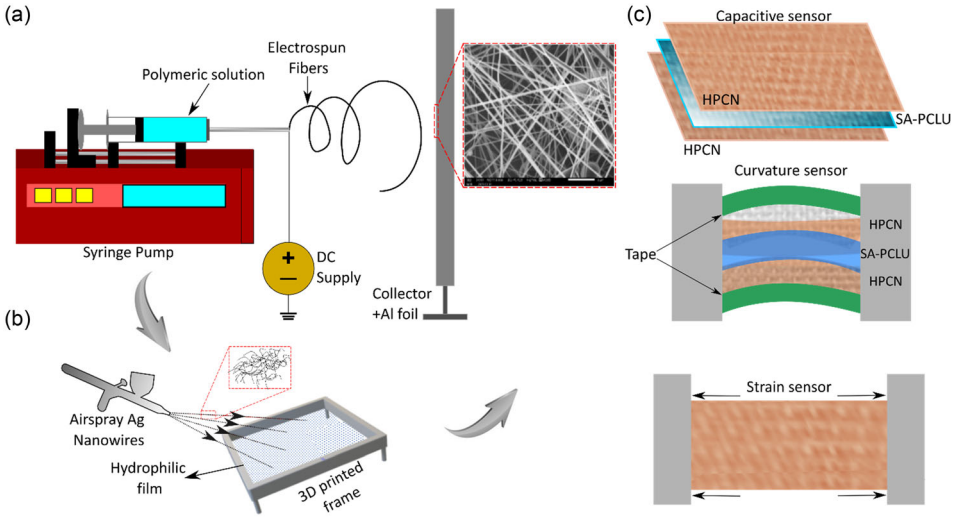

Figure 2. Pictorial presentation for the fabrication of the HPCN electrode and layout of a capacitive pressure sensor and strain sensors. a) Electrospinning of SA-PCLU, b) spraying Ag nanowires on SA-PCLU mounted on the 3D printed frame, and c) layout of the capacitive sensor, curvature sensor, and strain sensor.

silanediol and amine functionality. The hydrophilic surface of the SA-PCLU substrate has a strong affinity for Ag nanowires in water, allowing the Ag nanowires to spread more evenly and cover a larger surface area. The air spray not only uniformly disperses the Ag nanowires across the substrate surface but also provides the force needed for the Ag nanowires to penetrate the electrospun fibers. After drying the Ag nanowire-sprayed SA-PCLU films under ambient conditions, the HPCN is obtained as a freestanding, transparent, and stretchable conductive surface.

Figure 3a shows the top view of the scanning electron microscopy (SEM) image of the as-electrospun SA-PCLU fiber mat. The fibers are very smooth without any beads and orient to random directions due to the flat plate collector. Based on SEM images, the fiber diameters were measured and found to range from 300 to 900 nm, with an average diameter ≈450 from 100 points of diameter measured from the SEM and AFM images (Figure S2, Supporting Information). Different electrospinning parameters such as electrospinning voltage, solvents, and the weight/volume ratio led to different morphologies; the optimization table along with the corresponding SEM images is shown in Table S1 and Figure S3, Supporting Information respectively. Figure 3b shows the SEM images of the HPCN. The hydrophilic surface comprising the nanofibers acts as a backbone, while highly conductive Ag nanowires adhered to these fibers form a conductive network. As revealed by the top-down view of an SEM image in Figure 3b, the Ag nanowires are ≈70 nm in diameter and ≈40 µm in length. Due to the air pressure during the Ag nanowires spraying process and the intrinsic hydrophilic interactions, the Ag nanowires have penetrated through the nanofibers membrane and made the surface slightly conductive even on the backside, making the films conductive on both sides. Thus, it can be assumed that the Ag nanowire connections are reinforced by the fibers present in the scaffolds, and this is very important to the very good mechanical stability as discussed further in this manuscript. However, the spherical morphology observed in the inset of Figure 3b is due to the agglomeration of Ag nanowire clumps on the electrode surface, which is commonly seen when high aspect ratio nanowires (70 nm × 40 µm ($W \times L$)) are deposited on the substrate surface through air-spraying method.[50,51]

The as-fabricated HPCN surfaces also feature excellent homogeneity in the Ag nanowire deposition throughout the surface. As evidenced in Figure 3c, the presence of Ag is mapped via EDS mapping which reveals very good uniformity. In contrast, the control sample of electrospun poly(caprolactone) (PCL) showed no spreading of Ag nanowires in the ethanol:water droplets across the substrate, due to its hydrophobic character (Figure S4, Supporting Information). This merit is mainly attributed to the intrinsic hydrophilicity of the SA-PCLU film and uniformly dispersed Ag nanowires in water. Besides, the air spray method also ensures an even distribution of the Ag nanowire over the HPCN surfaces.

Further, the hydrophilicity of the SA-PCLU surface was also confirmed by contact angle measurements. The electrospun elastomer surface containing APTES displayed contact angle values of 59 ± 8° (refer to **Figure 4**a) as compared to the electrospun PCL surfaces (111.1 ± 0.1°) reported in the literature.[52] The hydrophilicity of the electrospun elastomer surface facilitated the air spray deposition of Ag nanowires during the fabrication of the HPCN. The resulting film on the surface was crucial for the uniform deposition of Ag nanowires across the surface.

The mechanical properties, such as elongation at break and tensile strength, are crucial for substrates as well as flexible electrodes used in flexible devices. The stress–strain profiles of the hydrophilic fabric substrate SA-PCLU, compared with HPCN, are shown in Figure 4b. The SA-PCLU surface can be easily extended under direct uniaxial stretching, showing a breaking elongation of ≈220% at a tensile strength of 5.2 KPa, which is better than other reported polycaprolactone-based electrospun surfaces.[53–55] In contrast, the HPCN exhibited a two-step breaking strain profile. The initial major breakage of the HPCN

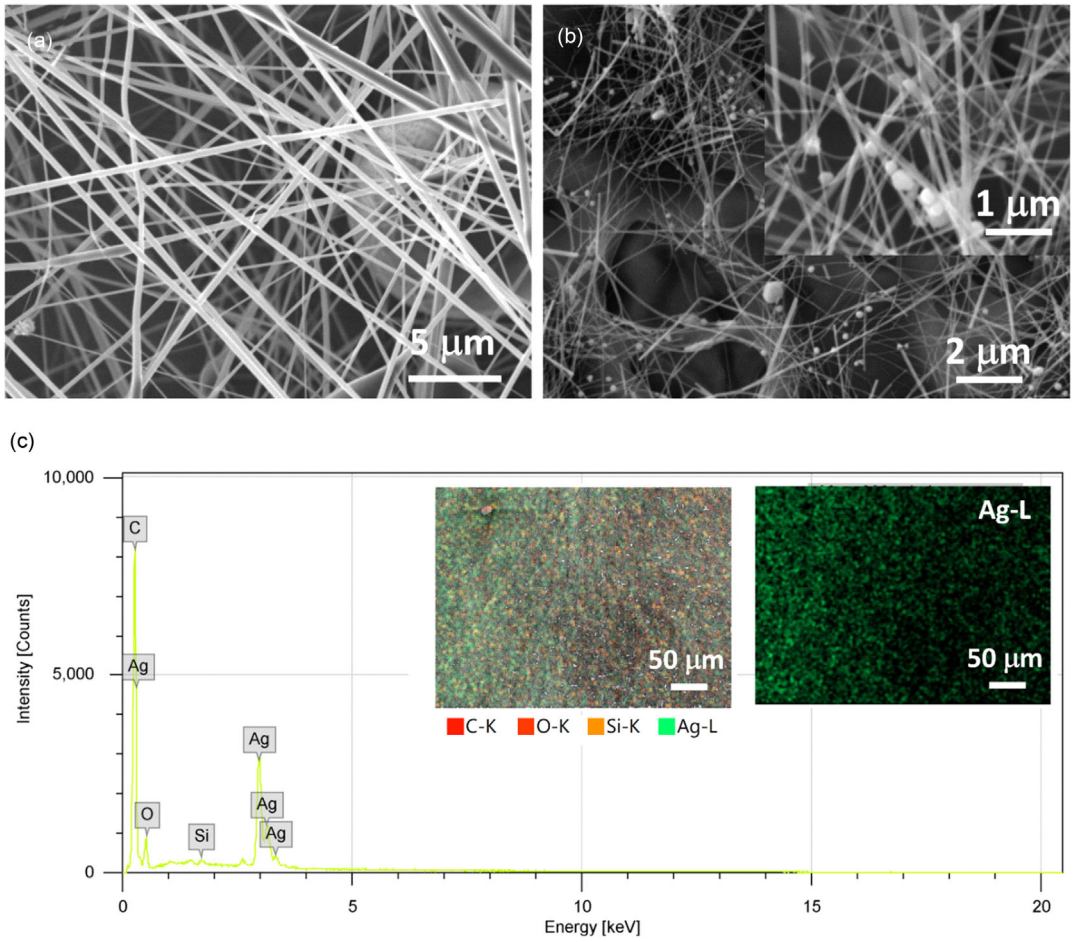

Figure 3. SEM images of a) electrospun SA-PCLU elastomer and b) HPCN electrode. c) The EDS spectra of the HPCN surface. The insets show the elemental mapping of the surfaces showing the uniform deposition of Ag nanowires across the HPCN surface.

occurred at 175% strain, followed by complete failure at more than 200% strain (Figure 4b). The differences in the stress–strain profile of HPCN compared to SA-PCLU may be due to the loaded AgNWs, which can either reinforce or embed on the elastomer surface. Loading AgNWs on the surface of electrospun fabric SA-PCLU makes the elastomer stiffer and less flexible due to the rigid metallic content, thus affecting the mechanical properties of the fabric elastomer. To further confirm the effect of Ag nanowires on the mechanical properties of SA-PCLU, we loaded various concentrations of Ag nanowires (10, 20, 30, 40, and 50 $\mu g\,cm^{-2}$) onto the SA-PCLU and studied its resilience properties at 5% strain over 3 cycles (Figure S5, Supporting Information). These studies reveal that the strain % decreased with each cycle as Ag nanowire loading increased, indicating that the material becomes less elastic and more rigid with higher AgNW content. Additionally, to evaluate the resilience of HPCN, we subjected the same film for mechanical testing under different strain loading conditions (10%, 20%, and 30%) for 20 cycles (Figure 4c). The results show that HPCN demonstrated rapid expansion and recovery under these conditions due to its low or negligible hysteresis. This property is critical for stretchable devices that undergo repeated mechanical deformations during stretching and bending.

Studying the stability of Ag nanowires on the electrode surface is crucial when the electrode is used as an e-skin sensor. To check the stability, the surface was dipped in the saline solution for 60 s and the resistance was recorded. The resistance only rises by $\approx$0.67% $cycle^{-1}$ average after 100 dipping cycles as shown in Figure 4d and might be due to the slight oxidation of Ag nanowires. A similar observation is also obtained if the saline solution is replaced by deionized water. Being immune to liquid interaction is solid evidence that the Ag nanowires are properly adhered and the HPCN electrode is promising to be adopted in electronic skins, as its conducting property is not compromised by commonly occurring external factors. For real-life applications such as for long-time exposure to heavy sweat, a thin layer of parylene-C may be coated onto the hydrophilic elastomer nanofibers by chemical vapor deposition or other methods, to further promote the chemical stability of the supporting electrospun surface.[56]

To assess the transparency of the HPCN, transmittance studies were conducted. The HPCN with a thickness of $\approx$300 μm was mounted onto the square-shaped 3D printed frame

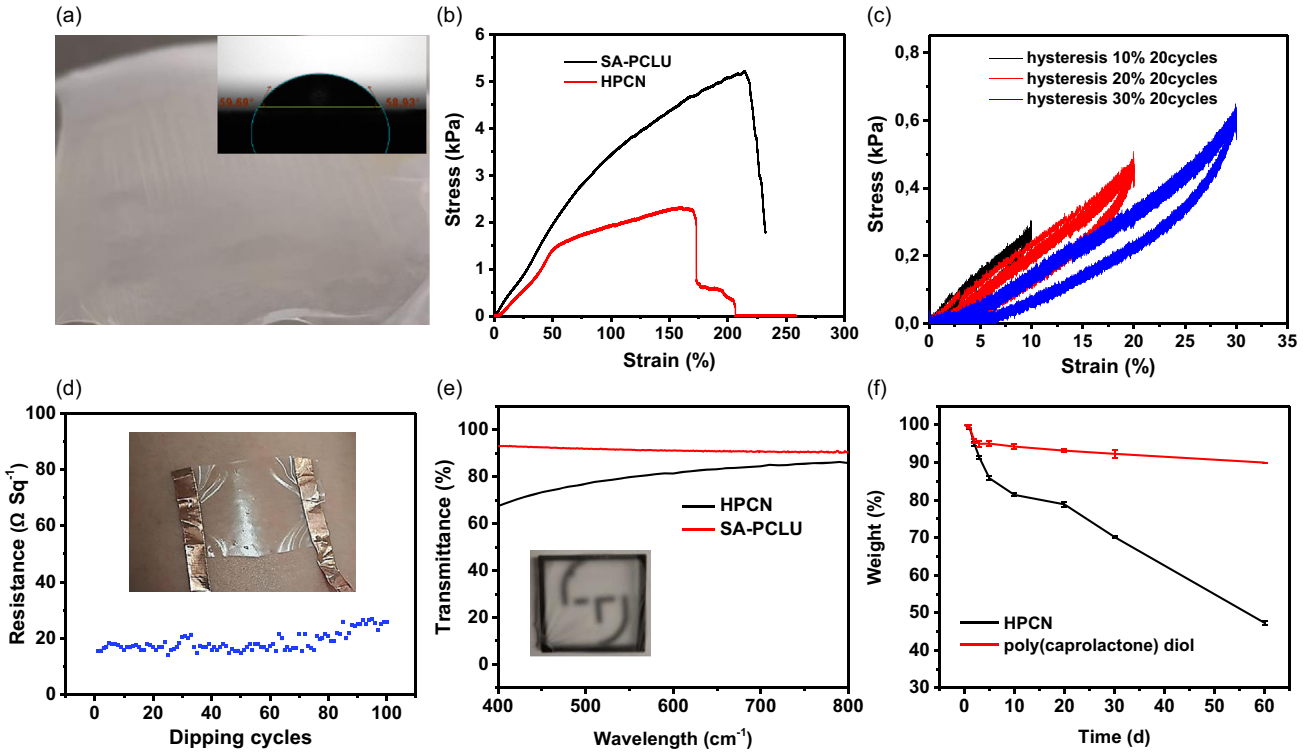

Figure 4. Characterization of SA-PCLU the electrospun hydrophilic film and HPCN electrode. a) Static contact angles of water on hydrophilic SA-PCLU elastomer film. The camera image shows the solution film (Ag nanowires in water) on the surface. b) Stress vs strain profile of the electrospun hydrophilic SA-PCLU elastomer surface and its HPCN electrode. c) Cyclic tensile studies of HPCN with 10%, 20%, and 30% strain over 20 cycles. d) Resistance measurement of the HPCN surface over 100 dipping cycles in saline solution. e) Relative transmittance spectra of the HPCN electrode (10 $\Omega\,sq^{-1}$) with the comparison of SA-PCLU. The inset shows the camera image of the SA-PCLU films mounted on the 3D-printed frame underneath the Tampere University logo. f) Degradation of the HPCN and control control PCL-diol over 60 days.

(dimensions: 1×1 inch), as depicted in Figure 4e. The results showed that the HPCN displayed an optical transmittance of nearly 82%, which is lower than the SA-PCLU film's transmittance of 90%. The reduced transmittance of HPCN compared to SA-PCLU is due to the light scattering caused by metallic Ag nanowires.[57,58] To demonstrate the material's potential use on skin, the target surface, specifically a human hand, was first moistened with water. Then, the HPCN surface was applied and allowed to dry, resulting in a uniform and conformal attachment to the skin. Due to the high transparency of the HPCN, the electrode on the skin was visible, as shown in the photograph in Figure 4d. The quantity of Ag nanowires loaded onto the surface directly affects the optical transmittance and conductivity of the material. The sheet resistance of the HPCN decreases significantly with increasing Ag nanowire loading, which has also been observed in other electrospun polymers containing Ag nanowires.[30] If the tentative loaded Ag nanowire concentration on the surface is $\approx 20\,\mu g\,cm^{-2}$, the sheet resistance ($R_s$) reaches as low as $\approx 10 \pm 3\,\Omega\,sq^{-1}$, which is comparable to most of the recently reported flexible electrodes.[30,59–61] For the conductive surfaces having a sheet resistance of $\approx 10\,\Omega\,sq^{-1}$, ≈82% transmittance is observed.

To demonstrate the degradability of the conductive surfaces, we immersed the sensor in a lipase solution and monitored its biodegradation over 60 days, as shown in Figure 4f. The results indicate significant degradation of the sensor over time. The degradation rate of the HPCN is much faster (nearly 53% degraded in 60 days) than that of the reference hydrophobic poly(caprolactone) diol (11% degraded in the same timeframe). The increased biodegradation of the hydrophilic HPCN in a lipase solution is primarily due to its higher affinity for water, leading to better swelling and increased surface area. This enhances enzyme accessibility and adsorption, facilitating more efficient enzymatic action and faster degradation compared to the hydrophobic parent poly(caprolactone) diol.[62–64] Based on the enzymatic degradation studies, we conclude that the conductive HPCN films are biodegradable and can be readily disposed of after serving their purpose as electrodes in flexible devices. It is noteworthy to mention that the toxicity of Ag nanowires is still not fully known; hence, nanowires based on other well-studied conductors such as Cu can also be integrated into the fabrication of conductive surfaces based on the electrospun HPCN.

The HPCN is highly flexible and stretchable, making it ideal for use in a range of tactile sensors. To create a capacitive pressure sensor, we layered a surface with Ag nanowires (loaded at $\approx 100\,\mu g\,mL^{-1}$) as the electrode with an electrospun hydrophilic elastomer surface without Ag nanowires on top (refer to Figure 2). As pressure is applied, the capacitance between the two electrodes changes, allowing us to measure and quantify

the pressure. We tested the sensor under a range of pressures from 0.01 to 63 kPa, as human skin typically experiences this range of pressures during normal activities. A mechanical tester with a 10 mm diameter cylindrical probe was used to progressively increase the pressure on the sensor. The capacitance was measured using an LCR meter while the weight on the sensor was increased stepwise, with the weight being entirely removed between each experiment. **Figure 5**a depicts the measured progressive capacitance change over time, and Figure 5b shows the same data plotted over pressure. We recorded several points in the low-pressure range (<10 kPa) to obtain an accurate estimation of the sensor's linearity in this regime. Typically, the sensitivity of sensors in modern applications is compared based on their response to a load. Using the values shown in Figure 5b, we can calculate the sensitivity (S) as a function of pressure (P) using the following equation.

$$S = \frac{d(C/C_0)}{dP} \tag{1}$$

Herein, the capacitance (C) of the sensor is measured and compared to the initial capacitance (C_0) when pressure (P) is applied. Figure 5b shows that the sensor's sensitivity is the highest when the pressure is the lowest. With increasing pressure, the sensitivity of the sensor tends to decrease dramatically since the sensor reaches its maximum measurable load point.

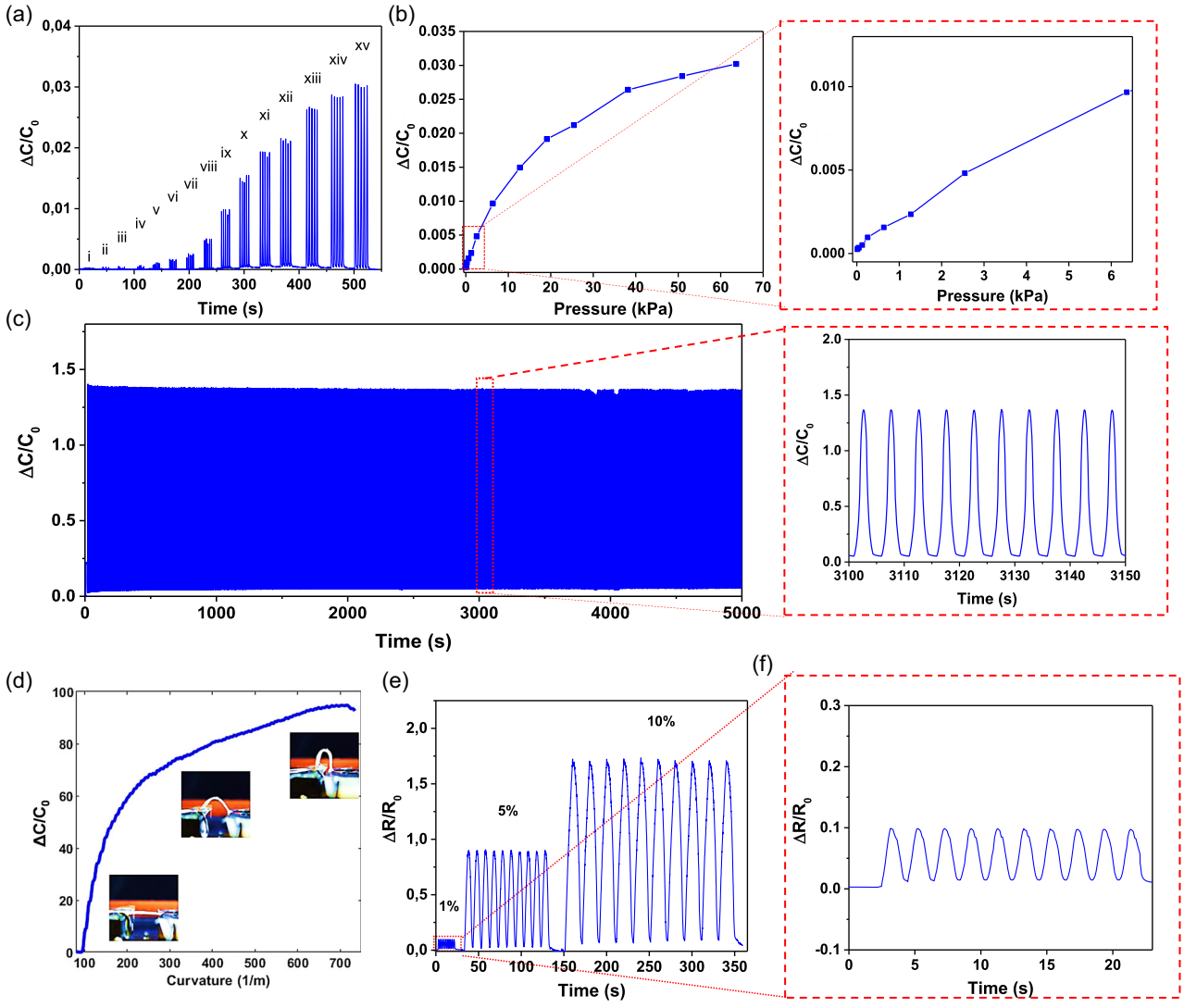

Figure 5. Characterization of the hydrophilic elastomer-based sensors: Capacitive sensor: a) Change in capacitance when the pressure is varied on the sensor from 0.01 to 63 kPa (i = 0.01273 kPa, ii = 0.02546 kPa, iii = 0.05093 kPa, iv = 0.12732 kPa, v = 0.25465 kPa, vi = 0.63662 kPa, vii = 1.27324 kPa, viii = 2.54647 kPa, ix = 6.36618 kPa, x = 12.73237 kPa, xi = 19.09855 kPa, xii = 25.46473 kPa, xiii = 38.1971 kPa, xiv = 50.92946 kPa, xv = 63.66183 kPa). b) Data from a, with relative capacitance, plotted as a function of the pressure, and a close-up of the low-pressure regime is taken from the graph shown in (b). c) The stability of the capacitive sensor when dynamically loaded for 1000 cycles with a pressure of 10 kPa. The close-up image shows the stability of the change in capacitance. Curvature sensor: d) The change in $\Delta C/C_0$ when the capacitive sensor was bent at different curvatures. The inset shows the camera images of the bending of the sensor. Strain sensor: e) The change in the $\Delta R/R_0$ for the sensor upon increase in the strain environments. f) The strain sensing in 1% strain.

Loading the sensor beyond its maximum pressure value could result in sensor failure, but in this case, the sensitivity progressively declined with increasing pressure. This sublinear response is advantageous as it provides a high dynamic range, as seen in previous reports. The sensor had a maximum sensitivity of $\approx 0.22\,kPa^{-1}$ in the low-pressure range, which is comparable to similar and recently reported electrospun capacitive sensors used in e-skin applications.[65–67]

The dynamic characteristics of the capacitive sensor used in this experiment are crucial, as it employs the same electrospun material. To assess these characteristics, a mechanical tester's probe was used to move up and down in a sinusoidal pattern. The sensor was subjected to a cyclic pressure of 10 kPa with a frequency of 0.2 Hz for 1000 cycles, and the results are presented in Figure 5c. While the sensor exhibited slight variations in signal intensity, the overall signal remained stable, as depicted in the inset of Figure 5c. It is noteworthy to mention that the elastomer is slightly sticky in nature (a hydrophilic silanol/amine-terminated monomaterial), which requires a few seconds to recover when subjected to higher loads. To confirm this, we calculated the specific electrical signal response time of the sensor by subjecting it to different applied pressures (1.27, 6.37, 12.73, and 63.66 kPa), corresponding to forces of 0.1, 0.5, 1, and 5 N, respectively. As shown in **Figure 6**, increasing the pressure on the sensor resulted in longer response times. The individual $\Delta C/C_0$ vs. time (s) profiles used to calculate the response times under different applied forces are provided in Figure S6, Supporting Information. This confirms that the sensor's slightly sticky nature causes a delay in recovery, leading to increased response time under higher pressure loads. To further verify this, a cyclic pressure test was conducted at a higher load of 20 kPa for 10 000 cycles at a frequency of 0.5 Hz (Figure S7, Supporting Information). The results showed increased signal intensity variations in the sensor, further supporting our hypothesis.

The HPCN surface has the potential to serve as a curvature sensor. The orientation of the sensor is illustrated in Figure 2, where a bare electrospun surface (without Ag nanowires) is placed between electrodes. The sensor is encapsulated in biodegradable transparent tape to prevent surface stretching and ensure repeated bending. To demonstrate the surface's effectiveness as a curvature sensor, the sensor was clamped at its edges and bent using a linear translation stage while measuring the curvature (using a digital camera and Image J) and the change in capacitance. Figure 5d displays a quadratic relation between ΔC and curvature, with values ranging from 0 to $700\,m^{-1}$. This process was repeated five times, and the results were averaged to obtain the calibrated capacitance. At $100\,m^{-1}$, the sensor displayed a relative capacitance value of 2 pF, while at $700\,m^{-1}$, the value was 95 pF.

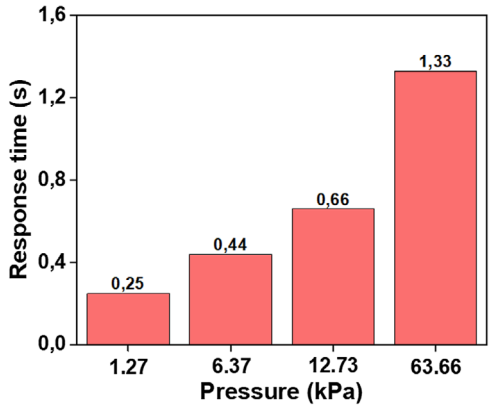

Figure 6. Sensor recovery response time at different applied forces (1.27, 6.37, 12.73, and 63.66 kPa).

The electrospun HPCN surfaces were utilized as strain sensors, with the ability to tolerate up to 15% strain (Figure 5e,f). These strain sensors possess stretchability, making them capable of full-range detection for applications such as electronic skins and human–machine interactive systems. To evaluate the strain-sensing properties, copper tapes were affixed to the two opposing edges of the HPCN surface, and the resistance change was monitored using an LCR meter while the surface was stretched using a mechanical tester under various loading conditions. The strain sensor displayed minimal overshoots when cyclically stretched up to 1%, 5%, 10%, and 15%, indicating low creep and reliable performance (Figure 5e,f). The sensing mechanism of the HPCN-based strain sensor is straightforward, where microstructural changes caused by applied strain led to variations in conductive paths and ultimately resistance. The resistance remained stable and repeatable until 10% strain but showed slight fluctuations beyond this range. However, a significant change in resistance occurred after 15% strain, and the values became erratic. It should be noted that soldering the Ag nanowires would enable the conductive surface to be utilized as a strain sensor at higher strains, as reported elsewhere[68,69]

The sensors based on the HPCN are proven to be very sensitive and can be used to detect the weak vibration of the sound speaker. The sensor was mounted onto the speaker as shown in **Figure 7**a. Figure 7b shows that capacitance variation outputs can be generated when the sensor based on HPCN is subjected to different vibrations at 20 dB. It is interesting to note that the sensor can also distinguish the vibration of different kinds of rock music. Drum tracks of rock music[70] with drumbeats ranging from 80 beats per minute (BPM) to 140 BPM were played which was detected as capacitance change with distinguishable variations. This indicates that the HPCN-based sensors are also suitable for mapping input vibrational signals.

The HPCN can be a crucial element in constructing electronic skins and is compatible with capacitive and curvature sensor-based e-skins. We demonstrated the practical applications of these sensors by affixing them to a hand to monitor human gestures (**Figure 8**a). Each of the five fingers on a nitrile glove used in the lab was equipped with a sensor to transform it into a smart glove for gesture monitoring. Different hand gestures were performed sequentially, with each gesture held for 20 s. The signal from each sensor reflected the gestures of each finger, as illustrated in Figure 8a. The signals were stable and repeatable, indicating that there was no delamination of the layers during the gesture monitoring experiments. The sensor was also demonstrated for capturing throat movements (Video SV2, Supporting Information). Throat movements can indicate when the test subject is breathing, speaking, or laughing, even in the absence of sound. This capability allows for the tracking of speech, even if the person cannot speak or must speak quietly.

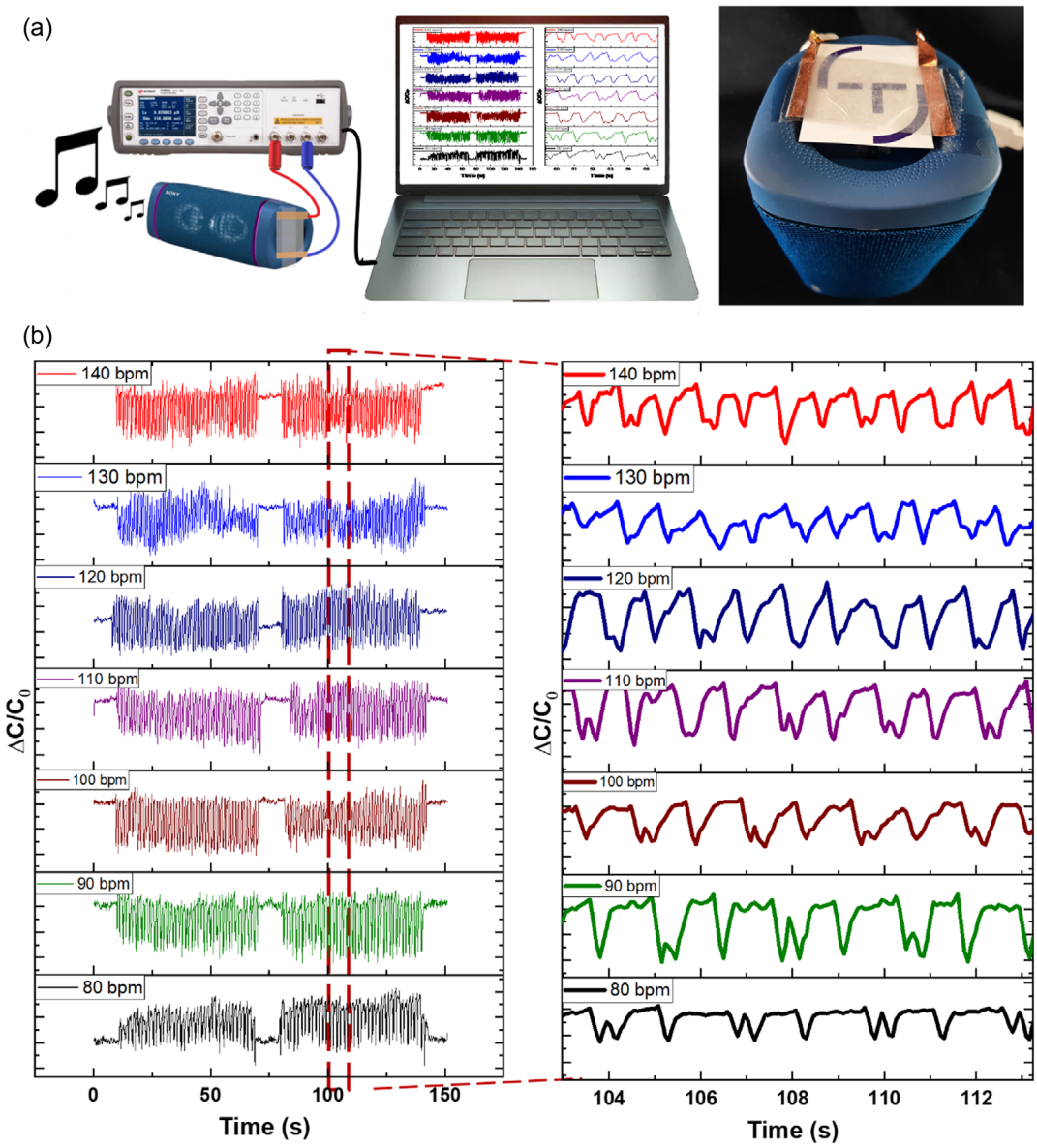

Figure 7. a) Schematic and camera image of the HPCN-based capacitive sensor mounted on the speaker. b) Capacitance variations response from the sensor when drum tracks of rock music with the drumbeats ranging from 80 to 140 BPM were played.

For the demonstration, the sensor was attached to the middle of the subject's neck, and the capacitance (C) was recorded while the subject was breathing normally, talking, and laughing. The sensor successfully distinguished different waveforms: low peaks signified breathing, high peaks indicated talking, and high, steep peaks represented laughing. This ability to detect various throat movements can be valuable for future applications requiring silent speech capture.

As the major application of flexible sensors and electrodes is in healthcare devices, we tested the feasibility of the HPCN-based capacitive sensors as swelling sensors. In many diseases like peripheral edema and various types of arthritis, the legs, hands, and other body parts swell due to the accumulation of excessive fluids. Edema or swelling in various body parts, however, can also be associated with more serious underlying medical conditions, such as diabetes, cardiac failure, and kidney disease. In many patients with chronic diseases, swelling is a crucial indicator of the onset or aggravation of the condition. Hence, swelling sensors might aid in monitoring and managing edema-causing diseases such as lymphedema, heart failure, kidney disease, diabetes, and venous insufficiency. The sensors can potentially detect fluid build-up, monitor fluid balance, and prevent foot ulcers. A proposed scheme of the utility of this sensor is shown in Figure 8b. As human trials were not possible, the HPCN-based swelling sensor was mounted onto the finger of the nitrile glove, and the air was filled slowly inside to mimic the real system. The swelling of the artificial finger was tracked as a function of capacitance change which is shown in Figure 8b.

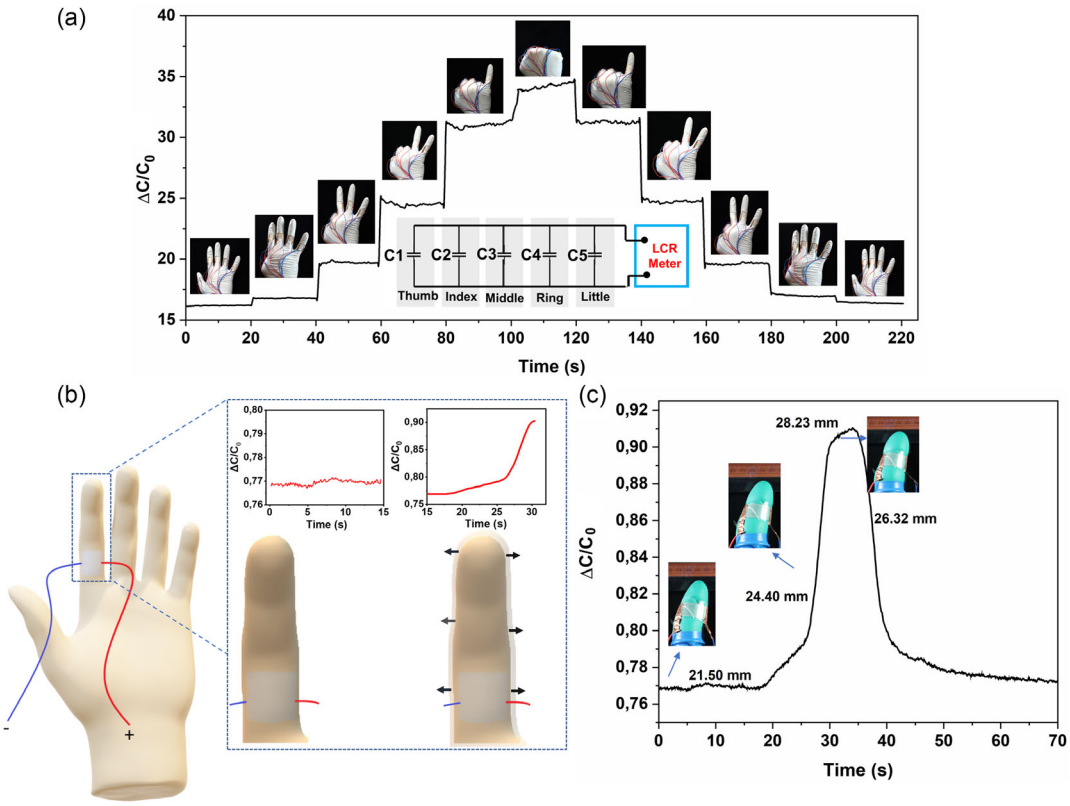

Figure 8. a) Sensor demonstration in gesture monitoring: Five sensors mounted on the hand, one on each finger. The sensor signals can be used to distinguish between different hand gestures. The inset shows the representative circuit diagram. b) Schematic of the HPCN-based capacitive sensor as a swelling sensor. c) The capacitance change when the glove's finger swells on filling the air in it. The inset shows the corresponding photographs.

Hence, it was proved that the sensors based on the HPCN can be used readily in monitoring the swelling. In addition, the porous structure of the electrode and the sensor allows the evaporation needed during perspiration. This makes it suitable to be used as a long-term use epidermal electrode.

Further, to evaluate the effect of skin friction on the conductive properties of the HPCN, we mounted the electrode on a human forearm and measured the sheet resistance after peeling it off at different time points: 0, 30 min, 1, 1.5, 2, 2.5, and 3 h. As shown in Figure S8, Supporting Information, the sheet resistance of the HPCN remained stable over time, indicating that the conductivity is not affected by friction with the skin. These findings suggest that the Ag nanowires are strongly adhered to the SA-PCLU substrate, enabling stable conductivity of the HPCN for long-term use on the skin without any fall-off of the Ag nanowires. Additionally, to evaluate the adhesive properties of the HPCN electrode, we employed a standard test setup using a texture analyzer and a cylindrical probe. A 3×1.5 cm HPCN film was attached to an aluminum foil substrate for testing. Due to its hydrophilic nature, the HPCN exhibited strong adhesion to the foil surface. A cylindrical probe (10 mm diameter) with double-sided tape was used to detach the HPCN from the foil. The force-displacement curve, shown in Figure S9, Supporting Information, demonstrates the adhesive strength during the detachment process, confirming the strong interaction between the HPCN and the aluminum substrate.

Overall, the characteristics of the HPCN electrode, such as transmittance (82%), sheet resistance (≈10 Ω sq^{-1}), biodegradability, sheet resistance over 100 saline dipping cycles, as well as its performance as a strain sensor under various applied strains (1–15%) and as a pressure sensor under a wide range of applied pressures (0.01–63 kPa) and curvatures (800 m^{-1}), were compared with several high-performance epidermal electrodes reported in the literature (Table S2, Supporting Information). The superior or comparable performance of our HPCN electrode, in comparison to these literature reports, makes it an excellent choice for various e-skin-based flexible strain, pressure, and swelling sensors.

3. Conclusions

We have synthesized degradable, transparent, stretchable, and breathable electrodes based on electrospun hydrophilic SA-PCLU elastomer. Ag nanowires dispersed in water were evenly distributed (using air spray) on the electrospun hydrophilic nanofibers. Owing to the intrinsic hydrophilicity of the surface, Ag nanowires adhere to it and spread evenly to the surface to obtain HPCN. The HPCN displayed very good stretchability (200%), breathability, optical transparency (≈82%), very good conductivity (≈10 Ω sq^{-1}), and good epidermal attachment. The HPCN electrodes were used in the

fabrication of capacitive sensors, curvature sensors, and resistive sensors. All these sensors are highly sensitive and can track a range of pressures, curvatures, and strains. The fully degradable nature of HPCN electrodes makes them an environmentally sustainable alternative to conventional electronic devices. The single-component system used in their production also simplifies the manufacturing process, reducing the environmental impact. The development of HPCN electrodes for use in capacitive sensors, curvature sensors, and resistive sensors could lead to significant advancements in healthcare technology. Electronic skins incorporating these sensors could be applied to monitor vital signs and detect abnormalities. The stretchability, breathability, and transparency of HPCN electrodes make them a promising material for various commercial applications, such as wearable technology and flexible displays.

4. Experimental Section

Materials: Polycaprolactone diol (PCL diol, MW = ≈2000 Daltons), isophorone diisocyanate, dibutyltin dilaurate (DBTDL, for synthesis), triethylene glycol (TEG, reagentplus, 99%), (3-aminopropyl)triethoxysilane (APTES), and N,N-dimethylformamide (DMF) were procured from Sigma–Aldrich and used as received. Solvents such as chloroform, ethanol, and methanol used were procured from VWR chemicals, Finland. For the fabrication of hydrophilic polyurethane-based (HPCN) electrode, Ag nanowires (aspect ratios 70 nm × 40 µm) in water were purchased from Sigma–Aldrich. For degradation experiments, lipase from *Rhizopus niveus* was ordered from Sigma–Aldrich.

Synthesis of Poly(Caprolactone-Urethane) Diol: The poly(caprolactone-urethane) diol was synthesized as per the published protocol.[71] In a typical procedure, poly(caprolactone)-diol (PCL-diol) (20 g, 1 eq, 0.01 mol) was placed in a 250 mL two-neck round-bottom flask and heated to melt at 80 °C under a constant nitrogen flow. Isophorone diisocyanate (4 g, 2 eq, 0.02 mol) was then added, and the reaction mixture was allowed for stirring 15 min. Subsequently, dibutyltin dilaurate (DBTDL) (12 mg, 0.05 w% relative to both monomers) was introduced into the reaction mixture and allowed the reaction mixture to stir at 80 °C for 3 h. Thereafter, the chain extender triethylene glycol (TEG) (0.85 g, 1 eq, 0.01 mol) was added into the reaction mixture in the anhydrous DMF (15 mL) and stirred the reaction mixture at the same temperature for the next 2 h. Upon completion of the reaction, DMF was removed using a rotary evaporator, and the resulting solid mass of poly(caprolactone-urethane) diol was purified by washing with n-heptane (30 mL × 4). The purified product was then dried in a rotavapor and in a vacuum-controlled oven at 50 °C.

Synthesis of Hydrophilic Silanol/Amine-Terminated Poly(Caprolactone-Urethane) Elastomer: The silanol/amine-terminated poly(caprolactone-urethane) (SA-PCLU) was synthesized by the silanization of poly (caprolactone-urethane) diol with (3-aminopropyl) triethoxysilane (APTES). Briefly, poly(caprolactone-urethane) diol (1 eq) in dry methanol was added by APTES (2.2 eq) and then the reaction mixture was allowed to stir at room temperature for 6 h. Thereafter, methanol:H_2O mixture (9:1) was added to the reaction mixture to hydrolyze the silyl ether in the functionalized APTES. Finally, the reaction mixture was dried in a rotary evaporator and the resultant SA-PCLU elastomer obtained was further purified by washing it with ethanol and vacuuming to dry in the rotavapor.

Procedure for the Electrospinning of SA-PCLU Fabric Film: In a standard procedure, the SA-PCLU elastomer (12 wt%) dissolved in chloroform: methanol mixture (1:1) was used for electrospinning. The elastomer nanofibers were produced using an electrospinning apparatus (Spinbox Systems by Bionica, Spain) with an applied positive voltage of 15 kV, a negative voltage of 2 kV, and a flow rate of 5 µL min^{-1} in a 10 mL syringe. A thin layer of the nanofabric SA-PCLU elastomer, serving as a peelable and free-standing substrate, was collected on the surface of hydrophobic Teflon-coated aluminum foil (Reynolds) wrapped around the flat metallic collector. Details of the electrospinning optimization parameters are provided in Table S1, Supporting Information.

Procedure for the Fabrication of the Hydrophilic Polyurethane-Based Conductive Network Electrode: The HPCN electrode was fabricated using a simple spray-coating method. In a typical procedure, the peeled electrospun fabric film of the elastomer was mounted on a 3D-printed frame (1 inch by 1 inch) and made conductive by spraying it with diluted Ag nanowires (100 µg mL^{-1}, aspect ratio 70 nm × 40 µm ($W \times L$)) dispersed in water. To ensure that most of the nanowire solution was sprayed uniformly onto the surface of the elastomer with minimal loss, the Ag nanowires were sprayed while maintaining a distance of ≈6 cm between the 3D-printed frame and the sprayer. The sprayed nanowire solution formed a uniform film on the surface, which was then allowed to dry under ambient conditions. The conductivity of the HPCN electrode was confirmed by measuring the resistance using a multimeter.

Procedure for Biodegradability Studies: In a standard procedure, thin films of the HPCN electrode (3 × 3 cm) and poly(caprolactone) diol (3 × 3 cm) were placed in sample glass Petri dishes and incubated at ambient temperature (37 °C). They were then treated with 10 mL of phosphate buffer solution mixed with 10 mg mL^{-1} of *Rhizopus niveus* lipase (≥1.5 U mg^{-1}; Mr ≈ 83 000). At specified time points (0, 1, 2, 3, 5, 10, 20, 30, and 60 days), the release medium was replaced with fresh medium. Changes in the weight of the polymer films were measured before and after degradation to determine the percentage of mass loss.

Characterization: Proton and carbon nuclear magnetic resonance (NMR) spectroscopy of the synthesized elastomer was recorded using a JEOL-500 MHz instrument (SCZ500R, JEOL Resonance, Japan) in deuterated chloroform ($CDCl_3$) with trimethylsilane (TMS) as the internal standard. Fourier transform infrared spectroscopy (FTIR) spectra were recorded using a PerkinElmer Spectrum One FTIR spectrophotometer (PerkinElmer, Waltham, MA). Water contact angle (CA) values were measured using the Attention Theta Lite optical tensiometer (Biolin Scientific Holding AB, Sweden) with the sessile drop method. Stress versus strain studies of the elastomeric substrate, as well as strain sensor measurements, were performed using a Universal Mechanical Tester (TA.XT Plus, Stable Micro Systems, Surrey, UK). For the capacitive sensor measurements, a cylindrical probe (Ø10 mm) was used to apply varying pressure, integrated with an LCR meter to measure the signal outputs. Differential scanning calorimeter (DSC) measurements were conducted using TA Instruments Q1000 (TA Instruments, New Castle, DE, USA). Thermogravimetric analysis (TGA) analysis was performed in 1000 °C mode, ramp-10° per minute spanning a temperature range from 30 to 800 °C under a nitrogen (N_2) atmosphere from TGA-Q-500 (TA Instruments, New Castle, DE, USA). A written consent was obtained from the participant regarding the research experiments related to the sensor demonstration.

Supporting Information

Supporting Information is available from the Wiley Online Library or from the author.

Acknowledgements

This work is supported by financial support from KONE Foundation (decision number 202012035), the Research Council of Finland (grant no. 331368), and project DURATRANS (364408, 2024–2027, under the framework of M-ERA.Net). The authors are thankful to the Materials Research Infrastructure (MARI) and Sustainable fabrication (SusFab) infrastructure at the University of Turku for infrastructural facilities.

Conflict of Interest

The authors declare no conflict of interest.

Author Contributions

Pulikanti Guruprasad Reddy: Conceptualization (supporting); Formal analysis (equal); Investigation (equal); Writing—review & editing (equal). **Vipul Sharma**: Conceptualization (lead); Data curation (lead); Formal analysis (lead); Funding acquisition (lead); Investigation (lead); Methodology (lead); Project administration (lead); Resources (lead); Validation (equal); Writing—original draft (lead); Writing—review & editing (equal). **Vijay Singh Parihar**: Conceptualization (supporting); Investigation (equal); Writing—original draft (supporting); Writing—review & editing (supporting). **Ijlal Haider**: Conceptualization (supporting); Formal analysis (supporting); Investigation (supporting); Methodology (supporting); Writing—original draft (supporting); Writing—review & editing (supporting). **Amit Barua**: Conceptualization (equal); Data curation (supporting); Writing—review & editing (supporting). **Anastasia Koivikko**: Data curation (supporting); Methodology (supporting); Writing—review & editing (supporting). **Kyriacos Yiannacou**: Investigation (supporting); Writing—review & editing (supporting). **Hatai Jongprasitkul**: Methodology (supporting). **Minna Kellomäki**: Writing—review & editing (supporting). **Veikko Sariola**: Methodology (supporting); Project administration (supporting); Writing—review & editing (supporting). **Pulikanti Guruprasad Reddy** and **Vipul Sharma** contributed equally to this work.

Data Availability Statement

The data that support the findings of this study are available from the corresponding author upon reasonable request.

Keywords

elastomers, electronic skins, flexible electronics, nanowires, polyurethanes

Received: July 19, 2024
Revised: September 20, 2024
Published online:

[1] D. Sengupta, J. Romano, A. Giri, P. Kottapalli, *npj Flexible Electron.* **2021**, *5*, 29.
[2] L. Lu, J. Zhang, Y. Xie, F. Gao, S. Xu, X. Wu, Z. Ye, *JMIR Mhealth Uhealth* **2020**, *8*, e18907.
[3] Y. Ni, Y. Wang, W. Xu, *Small* **2021**, *17*, 1905332.
[4] M. Wang, Y. Luo, T. Wang, C. Wan, L. Pan, S. Pan, K. He, A. Neo, X. Chen, K. He, A. Neo, X. Chen, *Adv. Mater.* **2020**, *33*, 2003014.
[5] Y. Yang, J. Han, J. Huang, J. Sun, Z. Lin Wang, S. Seo, Q. Sun, Y. Yang, J. Han, J. Huang, Z. L. Wang, Q. Sun, S. Seo, J. Sun, *Adv. Funct. Mater.* **2020**, *30*, 1909652.
[6] P. C. Uzabakiriho, M. Wang, C. Ma, G. Zhao, *Nanoscale* **2022**, *14*, 6600.
[7] Y. Jiang, F. Liang, H. Yang Li, X. Li, Y. Jun Fan, J. Wei Cao, Y. Ming Yin, Y. Wang, Z. Lin Wang, G. Zhu, *ACS Nano* **2022**, *16*, 746.
[8] Y. Peng, N. Yang, Q. Xu, Y. Dai, Z. Wang, *Sensors* **2021**, *21*, 5392.
[9] A. Kumar, *Sens. Actuators, A* **2022**, *344*, 113770.
[10] R. Tortelli, F. B. Rodrigues, E. J. Wild, *Parkinsonism Relat. Disord.* **2021**, *83*, 93.
[11] M. L. Frechette, B. M. Meyer, L. J. Tulipani, R. D. Gurchiek, R. S. Mcginnis, J. J. Sosnoff, *Curr. Neurol. Neurosci. Rep.* **2019**, *19*, 1.
[12] G. C. M. de Oliveira, J. H. D. S. Carvalho, L. C. Brazaca, N. C. S. Vieira, B. C. Janegitz, *Biosens. Bioelectron.* **2020**, *152*, 112016.
[13] I. Vanmechelen, H. Haberfehlner, J. De Vleeschhauwer, E. Van Wonterghem, H. Feys, K. Desloovere, J. M. Aerts, E. Monbaliu, *Front. Rob. AI* **2023**, *9*, 1068413.
[14] Y. G. Park, G. Y. Lee, J. Jang, S. M. Yun, E. Kim, J. U. Park, *Adv. Healthcare Mater.* **2021**, *10*, 2002280.
[15] H. Ullah, M. A. Wahab, G. Will, M. R. Karim, T. Pan, M. Gao, D. Lai, Y. Lin, M. H. Miraz, *Biosensors* **2022**, *12*, 630.
[16] W. Yang, Y. Qin, Z. Wang, T. Yu, Z. Ge, *J. Electron. Mater.* **2022**, *51*, 6735.
[17] D. Qi, Z. Liu, W. R. Leow, X. Chen, *MRS Bull.* **2017**, *42*, 103.
[18] M. Hassan, G. Abbas, N. Li, A. Afzal, Z. Haider, S. Ahmed, X. Xu, C. Pan, Z. Peng, M. Hassan, G. Abbas, N. Li, X. Xu, Z. Peng, A. Afzal, Z. Haider, S. Ahmed, *Adv. Mater. Technol.* **2022**, *7*, 2100773.
[19] K.-J. Baeg, J. Lee, J. K. Baeg, J. Lee, *Adv. Mater. Technol.* **2020**, *5*, 2000071.
[20] S. Chen, Z. Wu, C. Chu, Y. Ni, R. E. Neisiany, Z. You, *Adv. Sci.* **2022**, *9*, 2105146.
[21] X. Duan, W. Cao, X. He, M. Wang, R. Cong, Z. Zhang, C. Ning, C. Wang, S. Zhao, Z. Li, W. Gao, *Chem. Eng. J.* **2023**, *476*, 146536.
[22] C. Wang, X. Duan, X. Li, W. Pan, C. Ning, F. Wang, W. Cao, F. Ou, M. Wang, Q. Liang, W. Gao, Z. Li, S. Zhao, *Adv. Funct. Mater.* **2024**, *34*, 2402815, https://doi.org/10.1002/ADFM.202402815.
[23] C. Wang, K. Xia, H. Wang, X. Liang, Z. Yin, Y. Zhang, C. Y. Wang, K. L. Xia, H. M. Wang, X. P. Liang, Z. Yin, Y. Y. Zhang, *Adv. Mater.* **2018**, *31*, 1801072.
[24] T. Cheng, Y. Zhang, W.-Y. Lai, W. Huang, *Adv. Mater.* **2015**, *27*, 3349.
[25] Y. Chen, R. S. Carmichael, T. B. Carmichael, *ACS Appl. Mater. Interfaces* **2019**, *11*, 31210.
[26] D.-H. Kim, J. A. Rogers, *Adv. Mater.* **2007**, *20*, 4887.
[27] S. Liu, Y. Rao, H. Jang, P. Tan, N. Lu, *Matter* **2022**, *5*, 1104.
[28] Z. Fan, Y. Zhang, Q. Ma, F. Zhang, H. Fu, K. C. Hwang, Y. Huang, *Int. J. Solids Struct.* **2016**, *91*, 46.
[29] Y. J. Fan, P. T. Yu, F. Liang, X. Li, H. Y. Li, L. Liu, J. W. Cao, X. J. Zhao, Z. L. Wang, G. Zhu, *Nanoscale* **2020**, *12*, 16053.
[30] Y. J. Fan, X. Li, S. Y. Kuang, L. Zhang, Y. H. Chen, L. Liu, K. Zhang, S. W. Ma, F. Liang, T. Wu, Z. L. Wang, G. Zhu, *ACS Nano* **2018**, *12*, 9326.
[31] X. Yang, S. Wang, M. Liu, L. Li, Y. Zhao, Y. Wang, Y. Bai, Q. Lu, Z. Xiong, S. Feng, T. Zhang, X. Yang, S. Wang, M. Liu, L. Li, Y. Zhao, Y. Wang, Y. Bai, Q. Lu, Z. Xiong, S. Feng, T. Zhang, *Small* **2022**, *18*, 2106477.
[32] W. B. Han, G. J. Ko, K. G. Lee, D. Kim, J. H. Lee, S. M. Yang, D. J. Kim, J. W. Shin, T. M. Jang, S. Han, H. Zhou, H. Kang, J. H. Lim, K. Rajaram, H. Cheng, Y. D. Park, S. H. Kim, S. W. Hwang, *Nat. Commun.* **2023**, *14*, 2263.
[33] B. Ates, S. Koytepe, S. Balcioglu, M. G. Karaaslan, U. Kelestemur, S. Gulgen, O. Ozhan, *Int. J. Adhes. Adhes.* **2019**, *95*, 102396.
[34] E. Liu, Z. Cai, Y. Ye, M. Zhou, H. Liao, Y. Yi, *Sensors* **2023**, *23*, 817.
[35] W. Gao, S. Emaminejad, H. Yin, Y. Nyein, S. Challa, K. Chen, A. Peck, H. M. Fahad, H. Ota, H. Shiraki, D. Kiriya, D.-H. Lien, G. A. Brooks, R. W. Davis, A. Javey, *Nature* **2016**, *529*, 509.
[36] P. Peng, A. Hu, H. Huang, A. P. Gerlich, B. Zhao, Y. N. Zhou, *J. Mater. Chem.* **2012**, *22*, 12997.
[37] L. F. Gerlein, J. A. Benavides-Guerrero, S. G. Cloutier, *Sci. Rep.* **2021**, *11*, 24156.
[38] Z. Aytac, S. Ipek, I. Erol, E. Durgun, T. Uyar, *Colloids Surf., B* **2019**, *178*, 129.
[39] P. Guruprasad Reddy, A. J. Domb, *Polym. Adv. Technol.* **2021**, *32*, 3835.
[40] L. Xing, X. Wang, M. Li, Y. Jia, G. Yang, C. Liu, C. Shen, X. Liu, *Adv. Nanocompos.* **2024**, *1*, 171.
[41] L. Li, L. Han, H. Hu, R. Zhang, *Mater. Adv.* **2023**, *4*, 726.
[42] P. Guruprasad Reddy, A. Barua, T. Laukkanen, B. Mostafiz, T. Tirri, A. Vainio, V. Sharma, *Chem. Eng. J.* **2024**, *495*, 153531.
[43] D. Bodas, C. Khan-Malek, *Sens. Actuators, B* **2007**, *123*, 368.
[44] S. R. Gaboury, M. W. Urban, *J. Appl. Polym. Sci.* **1992**, *44*, 401.

[45] S. Breisch, B. De Heij, M. Löhr, M. Stelzle, *J. Micromech. Microeng.* **2004**, *14*, 497.
[46] J. Lai, B. Sunderland, J. Xue, S. Yan, W. Zhao, M. Folkard, B. D. Michael, Y. Wang, *Appl. Surf. Sci.* **2006**, *252*, 3375.
[47] D. M. Widjonarko, J. Jumina, I. Kartini, N. Nuryono, *Indones. J. Chem.* **2014**, *14*, 143.
[48] G. Zhao, X. Ma, Z. Shao, X. Huang, J. Huang, H. Luo, *J. Sol-Gel Sci. Technol.* **2023**, *106*, 518.
[49] Y. Gao, S. Bai, K. Zhu, X. Yuan, *J. Biomater. Sci., Polym. Ed.* **2024**, *35*, 1157.
[50] X. Feng, X. Wang, B. Zhang, J. Gu, C. Xu, S. Zhang, *J. Mater. Sci.: Mater. Electron.* **2022**, *33*, 25939.
[51] N. P. Kovalec, E. P. Kozhina, I. M. Doludenko, I. V. Razumovskaya, S. A. Bedin, Y. V. Grigoriev, V. M. Kanevsky, *Bull. Russ. Acad. Sci.: Phys.* **2021**, *85*, 854.
[52] M. Srikanth, R. Asmatulu, K. Cluff, L. Yao, *ACS Omega* **2019**, *4*, 5044.
[53] F. Croisier, A.-S. Duwez, C. Jérôme, A. F. Léonard, K. O. Van Der Werf, P. J. Dijkstra, M. L. Bennink, *Acta Biomater.* **2011**, *8*, 218.
[54] R. Yaseri, M. Fadaie, E. Mirzaei, H. Samadian, A. Ebrahiminezhad, *Sci. Rep.* **2023**, *13*, 9434.
[55] S. R. Baker, S. Banerjee, K. Bonin, M. Guthold, *Materials* **2015**, *8*, 3508.
[56] N. Chou, H. Moon, J. Park, S. Kim, *Prog. Org. Coat.* **2021**, *157*, 106309.
[57] X. Yu, X. Yu, J. Zhang, D. Zhang, J. Ni, H. Cai, D. Zhang, Y. Zhao, *Mater. Lett.* **2015**, *145*, 219.
[58] H. Lee, M. Kim, I. Kim, H. Lee, *Adv. Mater.* **2016**, *28*, 4541.
[59] S. Jung, M. Song, D.-G. Kim, D. S. You, J.-K. Kim, C. S. Kim, S. Lee, T.-M. Kim, K.-H. Kim, J.-J. Kim, O. Center, J.-W. Kang, S. Jung, S. Lee, M. Song, D.-G. Kim, S. You, J.-K. Kim, C. S. Kim, T.-M. Kim, K.-H. Kim, J.-J. Kim, J.-W. Kang, *Adv. Energy Mater.* **2014**, *4*, 1300474.
[60] D. Li, W.-Y. Lai, Y.-Z. Zhang, W. Huang, D. D. Li, Y. W. Lai, Y.-Z. Zhang, W. Huang, *Adv. Mater.* **2018**, *30*, 1704738.
[61] S. Huang, Y. Liu, Y. Zhao, Z. Ren, C. Fei Guo, S. Huang, C. F. Guo, Y. Zhao, Y. Liu, Z. Ren, *Adv. Funct. Mater.* **2019**, *29*, 1805924.
[62] M. Zarei, B. Michalkiewicz, M. El Fray, M. Zarei, M. El Fray, B. Michalkiewicz, *Macromol. Mater. Eng.* **2024**, *309*, 2300443.
[63] B. Laycock, M. Nikolić, J. M. Colwell, E. Gauthier, P. Halley, S. Bottle, G. George, *Prog. Polym. Sci.* **2017**, *71*, 144.
[64] P. G. Reddy, A. J. Domb, *Biomacromolecules* **2022**, *23*, 4959.
[65] X. Yang, Y. Wang, X. Qing, *Sens. Actuators, A* **2019**, *299*, 111579.
[66] M. F. Lin, C. Cheng, C. C. Yang, W. T. Hsiao, C. R. Yang, *Org. Electron.* **2021**, *98*, 106290.
[67] M. Su, J. Fu, Z. Liu, P. Li, G. Tai, P. Wang, L. Xie, X. Liu, X. He, D. Wei, J. Yang, *ACS Appl. Mater. Interfaces* **2023**, *15*, 48683.
[68] X. Hu, J. Feng, H. Zhang, J. Ma, Z. Wu, J. Wen, S. Wang, Y. Tian, *Adv. Mater. Technol.* **2023**, *8*, 2300759.
[69] D. Tan, C. Jiang, Q. Li, S. Bi, J. Song, *J. Mater. Sci.: Mater. Electron.* **2020**, *31*, 15669.
[70] (60) 80 BPM - ROCK - 4/4 Drum Track - Metronome - Drum Beat - YouTube, n.d., https://www.youtube.com/watch?v=KNu9h4MA32Q (accessed: October, 2024).
[71] H. Tran, V. R. Feig, K. Liu, H. C. Wu, R. Chen, J. Xu, K. Deisseroth, Z. Bao, *ACS Cent. Sci.* **2019**, *5*, 1884.